# The Five-Day Wave on a Sphere with Realistic Zonal Winds

J. E. GEISLER[1]

*Rosenstiel School of Marine and Atmospheric Sciences, University of Miami, Coral Gables, Fla. 33124*

ROBERT E. DICKINSON

*National Center for Atmospheric Research,[2] Boulder, Colo. 80303*

(Manuscript received 11 August 1975, in revised form 11 December 1975)

ABSTRACT

A 5-day zonal wavenumber 1 oscillation has been well-documented from analysis of surface pressure data, and it has been suggested that it corresponds to the gravest symmetric low-frequency external normal mode of the atmosphere. Previous discussions of such global normal modes have assumed a basic state atmosphere at rest. In this investigation we solve linearized equations governing this mode in an atmosphere with a realistic distribution of zonal winds and including the surface temperature gradient in the lower boundary condition. Time-dependent solutions are obtained for zonal wavenumber 1 on a sphere using finite differences in the latitude-altitude plane. The frequency of symmetric forcing at the lower boundary is varied to find the resonant frequency of the gravest mode. In the presence of solstice zonal winds there is a large latitudinal asymmetry in the response in the upper stratosphere and in the mesosphere. An important feature of this asymmetry is relatively large amplitudes in the summer mesosphere. The amplitude of the temperature wave in the summer mesosphere is 10 K if the amplitude of the solution is scaled to give agreement with surface pressure observations and dissipation by Newtonian cooling is included in the calculation. The period of the mode is very little changed from its value for a basic state atmosphere at rest due to the fact that zonal winds and the temperature gradient at the lower boundary produce almost equal but opposite changes in period. Cancellation of the effects of zonal winds and lower boundary temperature gradient also appears to be responsible for the absence of a significant hemispheric asymmetry in mode structure in the troposphere and lower stratosphere. The time required for the mode to respond completely to lower boundary forcing is on the order of a month.

## 1. Introduction

The linearized equations describing oscillations of a stratified resting atmosphere on a spherical earth can be separated into a latitudinal structure equation and vertical structure equation (Taylor, 1929). The former equation, which describes oscillations of an incompressible fluid of uniform depth on a sphere, is generally referred to as Laplace's tidal equation. The eigenfunctions of this equation, satisfying the boundary conditions that the disturbance vanish at the poles, have been calculated over an extensive parameter range by Longuet-Higgins (1968). At frequencies low compared to the angular rotation of the earth there exists a class of eigenfunctions whose phase propagation is only toward the west. In this paper we will be concerned with the member of this class of global Rossby modes that is of zone wavenumber 1 and of gravest symmetric latitudinal structure in the pressure field.

The *free oscillations* of the atmosphere necessarily satisfy the conditions that vertical velocity vanish at the ground and that vertically integrated energy be finite. In an isothermal atmosphere at rest there is only one solution of the vertical structure equation satisfying these conditions, and associated with it a unique value of the separation constant. The form of the solution is that which is characteristic of an edge wave or *external mode* in a stratified compressible fluid above a horizontal boundary. For such a mode, velocity and temperature fields increase exponentially with altitude but energy density decreases exponentially. With the value of the separation constant thus determined, the period of the gravest, symmetric, zonal wavenumber 1 Rossby mode is almost exactly 5 days. We refer to this global-scale external mode as the 5-day wave.

The best observational evidence for the 5-day wave is the study of Madden and Julian (1972). They computed cross spectra from time series of pressure data taken at stations distributed over the globe and isolated a zonal wavenumber 1 oscillation having no phase tilt with altitude and westward phase propagation with a period of about 5 days. From synoptic data they prepared a composite wave which showed maximum amplitude in middle latitudes and no phase shift between there and the equator. These are also features of the theoretical 5-day wave. In a sub-

[1] Presently on leave of absence to the National Science Foundation.

[2] The National Center for Atmospheric Research is sponsored by the National Science Foundation.

sequent paper (Madden and Julian, 1973) revising the composite wave, the amplitude of the surface pressure oscillation was estimated to be 0.5–1 mb in the tropics and 1–2 mb in middle latitudes. Preliminary results from a cross-spectral study of 73 years of subtropical data (Madden and Stokes, 1975) show the 5-day wave to be always present in the summer, but that it is more difficult to unambiguously identify in winter. These authors suggest that this may be a result of seasonal variation of the ratio of signal to noise. Rodgers (1976) reports evidence for these waves in the upper stratosphere.

According to the analysis of Tsay (1974), the 5-day wave is also present in the NCAR general circulation model. He spectrally analyzed data from a January simulation by the model and found a 5-day period, zonal wavenumber 1 oscillation in the wind and pressure whose latitudinal dependence looks very much like that of the theoretical 5-day wave. He also established that the phase of this oscillation is independent of altitude and that at 7.5 km in the model the maximum amplitude is 0.82 mb in middle latitudes. Extrapolating this figure down to the ground by means of the known altitude dependence of pressure fluctuations in an external mode, we arrive at a figure of about 2 mb for the maximum surface pressure oscillation, which is about the same as the amplitude deduced from observations by Madden and Julian (1973).

Since velocity and temperature fields in this external mode increase exponentially with altitude, the 5-day wave has potential significance for the upper atmosphere. This question has been looked at for acoustic-gravity external modes (Lamb modes) by Lindzen and Blake (1972), but similar calculations for Rossby wave external modes have not previously been done. The growth of fields with altitude in a stratified, compressible atmosphere is somewhat slower for these external modes than for internal modes. However, since the external modes are free oscillations, they should readily be generated by the transient and noisy character of the lower atmosphere.

As explained above, the 5-day wave has previously been interpreted only with models appropriate to an isothermal atmosphere at rest. In this investigation we solve approximate linear equations to find the period and structure of the 5-day wave in the presence of a realistic pattern of zonal winds over the globe. We find that the period of the oscillation is changed very little by the presence of zonal winds, which perhaps explains why the 5-day wave shows up in atmospheric data even though the zonal wind configuration is always changing. The structure of the 5-day wave in the troposphere is similarly affected very little by zonal winds. In the upper stratosphere and mesosphere, however, there is little resemblance between the structure in the presence of zonal winds and the external mode form of structure in the absence of zonal winds. Our model predicts a particularly large amplitude for the wave in the summer mesosphere.

## 2. Formulation of the model

We consider a small-amplitude disturbance of zonal wavenumber $s$ on a spherical earth situated in a zonal flow $\bar{u}$ that is a function of both latitude and altitude. The linearized primitive equations governing such a disturbance are

$$\left(\frac{\partial}{\partial t}+\frac{is\bar{u}}{a\cos\theta}\right)u'-\bar{Z}v'+w'\frac{\partial\bar{u}}{\partial z}=-\frac{isgh'}{a\cos\theta} \tag{1}$$

$$\left(\frac{\partial}{\partial t}+\frac{is\bar{u}}{a\cos\theta}\right)v'+\left[\bar{Z}+\frac{\cos\theta}{a}\frac{\partial}{\partial\theta}\left(\frac{\bar{u}}{\cos\theta}\right)\right]u'=-\frac{g}{a}\frac{\partial h'}{\partial\theta} \tag{2}$$

$$\left(\frac{\partial}{\partial t}+\frac{is\bar{u}}{a\cos\theta}\right)\frac{\partial h'}{\partial z}+\frac{R}{ga}\frac{\partial\bar{T}}{\partial\theta}v'+\kappa Hw'=0 \tag{3}$$

$$\frac{isu'}{a\cos\theta}+\frac{1}{a\cos\theta}\frac{\partial}{\partial\theta}(v'\cos\theta)+\frac{\partial w'}{\partial z}-w'=0. \tag{4}$$

In this set of equations a prime denotes perturbations and an overbar denotes mean quantities; $(u', v')$ = horizontal velocity components, $h'$ = perturbation height, $\theta$ = latitude, $z=\log(p_0/p)$ where $p_0$ is a reference pressure, $w'$ = vertical motion in this coordinate system, $a$ = radius of earth, $g$ = acceleration of gravity, $R$ = gas constant, and $\kappa=R/c_p$, where $c_p$ is the specific heat at constant pressure. The temperature field of the disturbance $T'$ is related to $h'$ by the hydrostatic equation $\partial h'/\partial z=(R/g)T'$.

Basic state parameters appearing in (1)–(3) are a temperature $\bar{T}$ related to $\bar{u}$ by thermal wind balance

$$\frac{\partial\bar{u}}{\partial z}=-\left(\frac{R}{2\Omega\sin\theta}\right)\frac{1}{a}\frac{\partial\bar{T}}{\partial\theta}, \tag{5}$$

and a basic state vorticity

$$\bar{Z}=2\Omega\sin\theta-\frac{1}{a\cos\theta}\frac{\partial}{\partial\theta}(\bar{u}\cos\theta), \tag{6}$$

where $\Omega$ is the angular rotation rate of the earth. An isothermal atmosphere characterized by scale height $H$ has been assumed in the evaluation of the static stability multiplying $w'$ in (3). It is believed that inclusion of realistic static stability variations (which would range by about a factor of 2) would introduce changes of a relatively minor nature compared to those due to realistic zonal winds (which have a much wider range).

It is convenient to transform to the variables $u$, $v$, $w$, $h$ defined by

$$(u', v', w', h')=(u,v,w,h)\exp(z/2) \tag{7}$$

and to introduce a streamfunction $\psi$ and velocity potential $\phi$ such that

$$\left.\begin{aligned} u&=\frac{is\phi}{a\cos\theta}-\frac{1}{a}\frac{\partial\psi}{\partial\theta}\\ v&=\frac{is\psi}{a\cos\theta}+\frac{1}{a}\frac{\partial\phi}{\partial\theta}\end{aligned}\right\}. \tag{8}$$

Multiplying Eq. (2) by $(is/a\cos\theta)$ and subtracting from this the result of operating on (1) with $(1/\cos\theta)\,\partial(\cos\theta)/\partial\theta$, we obtain the vorticity equation

$$\left(\frac{\partial}{\partial t}+\frac{is\bar{u}}{a\cos\theta}\right)\zeta=-\nabla\cdot\bar{Z}\nabla\phi-\frac{\partial\bar{Z}}{a\partial\theta}\left(\frac{is\psi}{a\cos\theta}\right), \tag{9}$$

where $\zeta$ is the vorticity of the $(u,v)$ field and is related to the streamfunction by

$$\zeta=\nabla^2\psi. \tag{10}$$

Multiplying Eq. (1) by $(is/a\cos\theta)$ and adding to this the result of operating on (2) with $(1/\cos\theta)\partial(\cos\theta)\partial\theta$, we obtain, after omitting certain terms to be described later, the following approximate form of the divergence equation:

$$\left(\frac{\partial}{\partial t}+\frac{is\bar{u}}{a\cos\theta}\right)\chi=\nabla\cdot\bar{Z}\nabla\psi-\nabla^2h. \tag{11}$$

Here $\chi$ is the horizontal divergence of the $(u,v)$ field and is related to the velocity potential by

$$\chi=\nabla^2\phi. \tag{12}$$

In these equations all $\nabla$ operators are those on a sphere but with the longitude derivative replaced by the quantity $is$.

We next operate on the thermodynamic equation (3) with $(\partial/\partial z-\frac{1}{2})$ after first transforming to the variables $h$, $v$, $w$ as given in (7). Eliminating $w$ from the resulting equation using (4), we obtain

$$\left(\frac{\partial}{\partial t}+\frac{is\bar{u}}{a\cos\theta}\right)\left(\frac{\partial^2}{\partial z^2}-\frac{1}{4}\right)h=\kappa H\chi+\frac{fv}{g}\left(\frac{\partial^2\bar{u}}{\partial z^2}-\frac{\partial\bar{u}}{\partial z}\right)+\frac{\partial\bar{u}}{\partial z}\left(\frac{\partial}{\partial z}-\frac{1}{2}\right)\left[\frac{fv}{g}-\frac{ish}{a\cos\theta}\right]. \tag{13}$$

In this investigation we solve the initial value problem with Eqs. (9), (11) and (13) regarded as predictive equations for $\psi$, $\chi$ and $h$. The motions of interest are characterized by large vertical scales on the order of an atmosphere scale height. Such motions are quasi-nondivergent everywhere on the sphere. Details of the appropriate scale analysis of the full divergence equation are given in Holton (1975). We let Ro denote the usual Rossby number $(=U/2\Omega L)$, where $U$ and $L$ are horizontal velocity and length scales of the motion), assumed $\ll 1$. Then the divergence equation correct to O(Ro) reduces to a balance between the two terms on the right-hand side of (11). All O(Ro) terms have thus been dropped in writing the divergence equation in the form (11). This cannot be justified *a priori* very close to the equator, where $\nabla\cdot\bar{Z}\nabla\psi$ itself becomes O(Ro). We retain the left-hand side of (11) even though it is O(Ro$^2$) for quasi-nondivergent motions since our method of solution depends on (11) being a predictive equation for $\chi$. Finally we drop the third term on the right-hand side of (13) because the term in brackets is O(Ro).

Boundary conditions at the upper and lower boundaries depend on the vertical velocity, that is, the vertical motion in the system where altitude is the vertical coordinate. Vertical velocity on a constant pressure boundary surface is taken to be the same as vertical velocity on a constant altitude boundary surface consistent with our linearization and neglecting topographic effects. We let $W'$ denote vertical velocity, and $w'$ the vertical motion in the coordinate system where $z=\log(p_0/p)$ is the vertical coordinate. An equation for the boundary condition is obtained from the definition $W'=Dh/Dt$, where $D/Dt$ is the convective derivative. When $D/Dt$ is evaluated in the log pressure coordinate system, this equation is

$$\left(\frac{\partial}{\partial t}+\frac{is\bar{u}}{a\cos\theta}\right)h'+\frac{v'}{a}\frac{\partial\bar{h}}{\partial\theta}+w'\frac{\partial\bar{h}}{\partial z}=W', \tag{14}$$

where $\bar{h}$ is the basic state geopotential height field. Consistent with the evaluation of static stability in the thermodynamic equation (3), we use the isothermal basic state height field to evaluate $\partial\bar{h}/\partial z$ in (14). Using also the fact that $\partial\bar{h}/\partial\theta$ is related geostrophically to $\bar{u}$, we can write (14) as

$$\left(\frac{\partial}{\partial t}+\frac{is\bar{u}}{a\cos\theta}\right)h'-\left(\frac{2\Omega}{g}\sin\theta\bar{u}\right)v'+Hw'=W'. \tag{15}$$

If we now eliminate $w'$ from this equation using the thermodynamic equation (3), we obtain, after transformation to the unprimed variables defined in (7),

$$\left(\frac{\partial}{\partial t}+\frac{is\bar{u}}{a\cos\theta}\right)\left(\frac{\partial}{\partial z}+\frac{1}{2}-\kappa\right)h+\left[\frac{\kappa}{g}(2\Omega\sin\theta)\bar{u}+\frac{R}{ga}\left(\frac{\partial\bar{T}}{\partial\theta}\right)\right]v=-\kappa W. \tag{16}$$

The term in brackets is proportional to the meridional gradient of basic state potential temperature at the boundary, as can be shown by differentiating the definition of potential temperature and expressing the pressure gradient in terms of $\bar{u}$. For a lower boundary

condition we use (16) with $W$ prescribed as a forcing function. Resonance modes satisfy the lower boundary condition $W=0$ and grow without limit if forcing at the boundary is applied at the resonance frequency. For convenience at the upper boundary we take $W=0$, corresponding to a rigid lid there. The form of the top boundary condition is unimportant provided the energy of solutions is small at the boundary compared to its typical value in regions of interest. Whether this is true will be examined latter.

A semi-implicit scheme (Robert, 1969; Robert *et al.*, 1972) is used for finite differencing in time. Let superscripts $+$ and $-$ denote quantities evaluated at $t\pm\Delta t$ and let the absence of a superscript denote a quantity evaluated at $t$. We now introduce the quantity $\hat{h}$ defined by

$$\hat{h}=\frac{h^{+}+h^{-}}{2} \tag{17}$$

in terms of which a time derivative will be given by

$$\frac{\partial h}{\partial t}\rightarrow\frac{\hat{h}-h^{-}}{\Delta t}.$$

We write Eqs. (9), (11) and (13) as

$$\hat{\zeta}=\zeta^{-}-\Delta t\left[\frac{is\bar{u}}{a\cos\theta}\zeta+\nabla\cdot\bar{Z}\nabla\phi+\frac{1}{a}\frac{\partial\bar{Z}}{\partial\theta}\left(\frac{is\psi}{a\cos\theta}\right)\right], \tag{18}$$

$$\hat{\chi}=\chi^{-}-\Delta t\left[\frac{is\bar{u}}{a\cos\theta}\chi+\nabla^{2}\hat{h}-\nabla\cdot\bar{Z}\nabla\psi\right], \tag{19}$$

$$\left(\frac{\partial^{2}}{\partial z^{2}}-\frac{1}{4}\right)\hat{h}=\left(\frac{\partial^{2}}{\partial z^{2}}-\frac{1}{4}\right)h^{-}$$

$$+\Delta t\left[\frac{-is\bar{u}}{a\cos\theta}\left(\frac{\partial^{2}}{\partial z^{2}}-\frac{1}{4}\right)h+\frac{fv}{g}\left(\frac{\partial^{2}\bar{u}}{\partial z^{2}}-\frac{\partial\bar{u}}{\partial z}\right)+\kappa H\hat{\chi}\right]. \tag{20}$$

The boundary equation (16) is

$$\left(\frac{\partial}{\partial z}+\frac{1}{2}-\kappa\right)\hat{h}=\left(\frac{\partial}{\partial z}+\frac{1}{2}-\kappa\right)h^{-}-\Delta t\left\{\frac{is\bar{u}}{a\cos\theta}\left(\frac{\partial}{\partial z}+\frac{1}{2}-\kappa\right)h\right.$$

$$\left.+\left[\frac{\kappa}{g}(2\Omega\sin\theta)\bar{u}+\frac{R}{ga}\left(\frac{\partial\bar{T}}{\partial\theta}\right)\right]v+\kappa W\right\}. \tag{21}$$

Solution of these equations proceeds in the following order, assuming that we have at hand $h$, $h^{-}$, $\chi$, $\chi^{-}$, $\zeta$, $\zeta^{-}$, $\psi$, $\psi^{-}$, $\phi$, $\phi^{-}$ (chosen to be zero at the initial time step). Using (19) we eliminate the divergence $\hat{\chi}$ from (20) so that it becomes a partial differential equation for $\hat{h}$ in the $(\theta,z)$ plane. This is solved using a block-tridiagonal matrix inversion. With this value of $\hat{h}$ we solve (19) for $\hat{\chi}$ and then solve (18) for $\hat{\zeta}$. From these we obtain $h^{+}$, $\chi^{+}$ and $\zeta^{+}$. Eqs. (10) and (12) are inverted to give $\psi^{+}$ and $\phi^{+}$. Boundary conditions in $\theta$ are that $h$, $\psi$, $\phi$ all go to zero at the poles. Centered differences are used for space derivatives with $\Delta\theta=15°$ and $\Delta z=6/7$. We adopt a value of 7 km for the isothermal atmosphere scale height, in which case the vertical grid point spacing is 6 km. With this coarse grid we are able to reproduce the known structure of the relevant external mode in the absence of zonal winds, including the velocity fields obtained by numerical differentiation of the streamfunction and velocity potential. Solutions with a time step $\leqslant 1$ h are found to be computationally stable.

Since the foregoing equations describe a wide spectrum of motions on a sphere, it is necessary to develop a forcing function that will excite only the desired mode. One consideration in this regard is that the latitudinal structure of the forcing function be such that it projects largely onto that mode. With this in mind we let the latitude dependence of the forcing function be that of the known solution in the absence of zonal winds (i.e., a Hough function), which can be estimated from Fig. 10 of Longuet-Higgins (1968). Later tests showed that the results obtained are not sensitive to the exact shape of the forcing, the same solution being obtained at large time for forcing with broad Gaussian latitude dependence. A further consideration is that the forcing must be turned on gradually and continuously so that the amplitudes of transient gravity wave modes are acceptably small. We found by trial and error that the forcing must increase on a time scale of not less than 10 days to accomplish this. Unavoidably excited even with this gradual forcing (and either with or without zonal winds) are very low frequency Rossby modes, particularly the first internal mode having similar latitudinal structure as the external mode we are seeking and physically spurious since its existence is due to an artificial top boundary condition. If the external mode is excited by gradually turning the forcing on and then off again, it is inextricably mixed with the first internal mode. To overcome this difficulty, we force continuously at a frequency close to that of the external mode so that its amplitude grows with time to become much larger than that of the internal mode.

The zonal wind model used is that of Lindzen and Hong (1974). These authors fitted observed zonally averaged temperatures with an analytic expression, then used surface winds and the thermal wind equation to obtain a global pattern of zonal winds. In this calculation we used the Lindzen and Hong solstice winds, shown in Fig. 1, and the associated distribution of temperature $\bar{T}$ at the lower boundary, shown in Fig. 2. Originally designed for a study of the effect of zonal winds on the vertical structure of atmospheric tides, this model underestimates somewhat the strength of horizontal and vertical shears in the tropospheric jets. It does, however, offer the outstanding advantage that it can be smoothly differentiated to

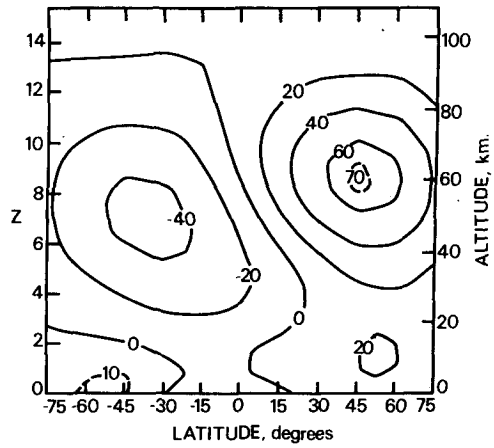


FIG. 1. Solstice zonal winds (m $s^{-1}$ calculated from the parameterization given in Lindzen and Hong (1974). Here and in subsequent figures positive latitude denotes the winter hemisphere. Conversion between altitude and the log pressure coordinate $Z$ is for an isothermal basic state atmosphere with 7 km scale height.

obtain the first and second derivatives of zonal winds that appear in the coefficients of our governing equations. Although it does not enter the equations as such, we show for reference in Fig. 3 the potential vorticity gradient

$$\frac{\partial \bar{q}}{a\partial\theta}=\left[\frac{\partial \bar{Z}}{a\partial\theta}-\frac{(2\Omega\sin\theta)^2}{\kappa g H}\left(\frac{\partial^2\bar{u}}{\partial z^2}-\frac{\partial\bar{u}}{\partial z}\right)\right] \tag{22}$$

evaluated for the solstice zonal winds and normalized by multiplying by $a/2\Omega$. In the absence of zonal winds, the contours in Fig. 3 would be those of $\cos\theta$, independent of altitude and having maximum value of unity at the equator.

Lindzen and Hong (1974) also gave a parameterization for equinox zonal winds. In contrast to the solstice model (Fig. 1) the equinox model has westerly wind jets of 32 m $s^{-1}$ at about 70 km, an easterly jet

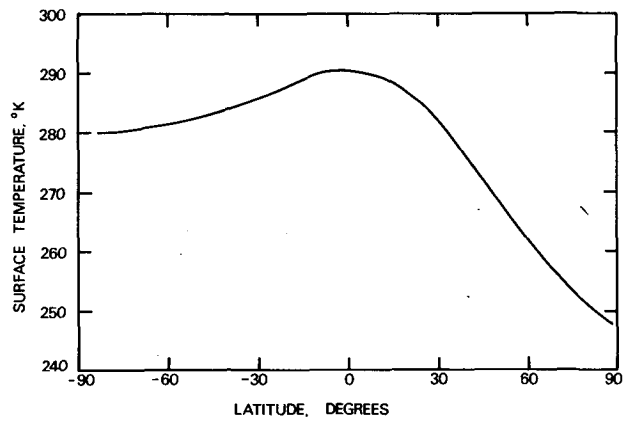


FIG. 2. Temperature at the lower boundary for the zonal wind distribution in Fig. 1, as calculated from the temperature parameterization given in Lindzen and Hong (1974).

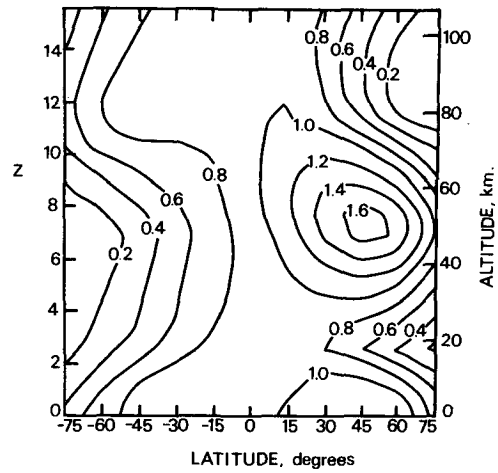


FIG. 3. Potential vorticity gradient calculated by numerically differentiating the zonal winds in Fig. 1 and nondimensionalized by multiplying by $a/2\Omega$.

of 14 m $s^{-1}$ centered at the equator, and westerly jets of 14 m $s^{-1}$ in the troposphere. Our calculated 5-day wave in this zonal wind model shows some features that distinguish it from the 5-day wave in the absence of zonal winds, which we comment on later. These differences, however, are not very significant as compared to the differences between the wave in solstice zonal winds and no zonal winds. We therefore present and discuss in detail only the results for solstice zonal winds.

## 3. Discussion of results

In the absence of zonal winds the equations governing the 5-day wave are separable The solution of the vertical structure equation for the height field variable $h$ of Eq. (7) is $\exp[(\kappa-\frac{1}{2})z]$, where $\kappa=2/7$. We have assumed an isothermal atmosphere with a scale height of 7 km, in which case the equivalent depth (proportional to the separation constant) is 9.8 km. With this value of equivalent depth Fig. 2 of Longuet-Higgins (1968) indicates that the period of the gravest symmetric wavenumber 1 Rossby mode is 5.0 days. The shape of the Hough function latitudinal structure for the mode can be inferred from Fig. 10 of that paper.

To illustrate the method of solution we follow in some detail the model calculation of the mode in the absence of zonal wind. Some features of this numerical solution are then checked against the known solution just described. We then present and discuss results for the model calculation of the mode in the presence of zonal winds.

At the initial time we introduce a vertical velocity at the ground with prescribed latitude dependence and with amplitude that grows slowly to a constant value as $1-\exp[-(t/T)^2]$, where $T=15$ days. The phase of the forcing depends on longitude and time

as $\exp[i(\lambda-\omega t)]$, where the angular frequency $\omega$ is chosen by trial and error to be arbitrarily close to the free mode frequency. The procedure for finding this frequency can be visualized with the aid of Fig. 4, which shows the phase of the solution at the ground as seen in a frame of reference rotating with the angular frequency $\omega$ of the forcing function. The curves are labelled by the period $(2\pi/\omega)$ of the forcing function. When, for example, this is longer than the period of the free mode, the phase of the solution advances in phase with time because the free mode is travelling westward faster than the reference frame. According to Fig. 4 the period of the free mode in the absence of zonal winds is about 5.4 days. By this technique we can estimate mode period to within $\pm 0.05$ day. We remark here that within these limits there is virtually no difference in the structure of the solution.

The time-dependent behavior of the solution with the 5.38-day forcing period is illustrated in Fig. 5, where we show phase at the top and bottom of the model at the equator and also the ratio of amplitude at these two points. The phase difference approaches zero and the amplitude ratio approaches a value close to 0.038, in agreement with the known vertical structure of the mode. Not illustrated in Fig. 5 is the fact that the solution grows with time because of the continuous forcing near a resonant frequency. The oscillation seen in Fig. 5 having a period of about 40 days is the first *internal* free mode having the same latitudinal structure as the external free mode we are considering. This internal mode has relatively large amplitude at the top of the model, but does not grow with time and therefore appears to damp out in Fig. 5. When the internal mode oscillation in Fig. 5 is conceptually filtered out, the behavior of the curves suggests that the external mode is set up on a time scale

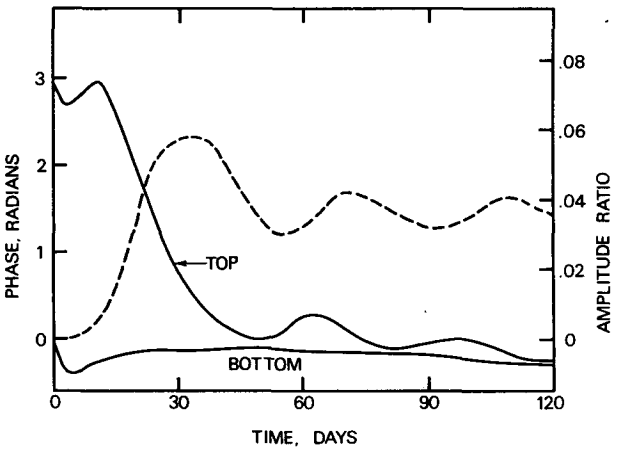


FIG. 5. Phase of $h$ at the top and at the bottom of the model at the equator in a reference frame travelling with the forcing (solid curves) and the ratio of the amplitude of $h$ at these two points (broken curve). Case shown here is for no zonal wind.

of about 30 days. Results shown subsequently are for 60 days of model time, beyond which time the solution is essentially the same apart from a scale factor linearly dependent on time. In all cases we normalize the results such that the maximum height field disturbance at the ground is 10 m, corresponding to maximum surface pressure perturbation of about 1 mb.

Fig. 6 shows the amplitude (m) of the geopotential height field variable $h$ [Eq. (7)] and accompanying temperature field for the mode in the absence of zonal winds at 60 days model time. As noted earlier, the period of the mode is 5.4 days. The vertical structure of $h$ in Fig. 6 agrees with the known vertical structure function $\exp[(\kappa-\frac{1}{2})z]$, and the latitudinal structure has the shape of the appropriate Hough function in-

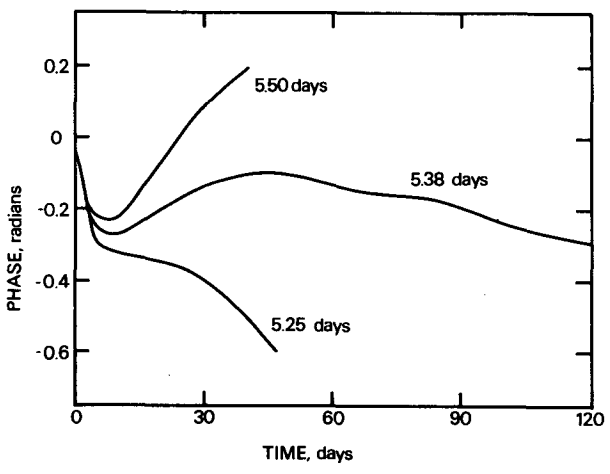


FIG. 4. Phase of the solution as a function of time in a reference frame rotating with the forcing. Curves are labelled according to the period of the forcing. The solution variable is $h$, related to perturbation height $h'$ by the definition $h=h'\exp(z/2)$.

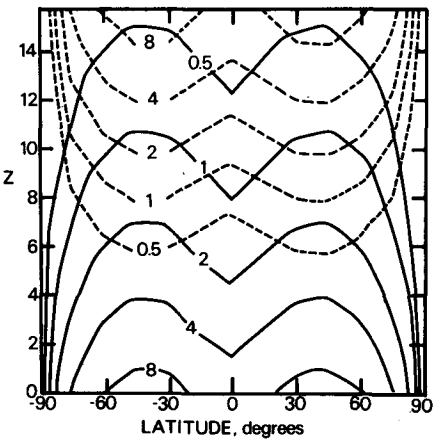


FIG. 6. Amplitude (m) of $h$ i.e., product of geopotential height and square root of pressure, in the case of no zonal wind (solid contours). In this and subsequent figures the solution has been normalized so that the maximum geopotential height disturbance at the ground is 10 m. Also amplitude (°K) of the temperature field in the case of no zonal wind (dashed contours).

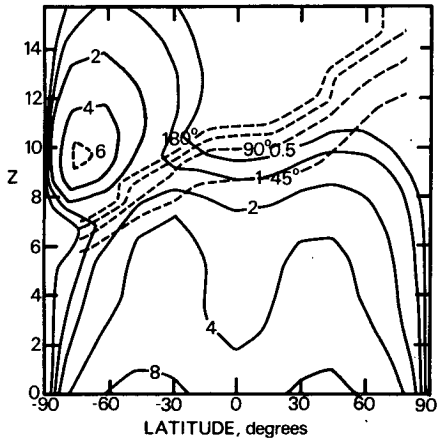


FIG. 7. Amplitude (m) of $h$ in solstice zonal winds (solid contours) and phase of $h$ in solstice zonal winds (dashed contours).

ferred from Fig. 10 of Longuet-Higgins (1968). The temperature field and the wave velocity field (the latter not shown) grow in the vertical as $\exp(\kappa z)$.

There is a discrepancy between the 5.0 day period obtained by the method described in the opening paragraph of this section and the $5.40 \pm 0.05$ day period obtained with the model. This is due to our use of the approximate form (11) for the divergence equation. For the case of no zonal winds this approximation consists of the neglect of a term involving the northward transport of the mean vorticity by the divergent component of motion. When this term is retained in the divergence equation, the period of the mode is changed to 4.95 days. Moura (1976) first noted the effect of omitting this term on phase velocities. Changes in mode structure with this term, on the other hand, are rather insignificant, amplitudes being very slightly larger in high latitudes and very slightly smaller near the equator. Similar small changes in amplitude occur when this term is included in the calculation of the mode in the presence of zonal winds. The difference between mode phase speeds with and without this term in the presence of mean winds is essentially the same as that found without winds. Thus the only notable consequence of omitting this term in the model equations, as we have done here, is roughly a 10% overestimate of mode period in all cases.

Fig. 7 shows the amplitude and phase of the mode when the global distribution of zonal winds is that shown in Fig. 1 and the corresponding temperature gradient (Fig. 2) is included in the lower boundary condition. For this calculation we use the same forcing function as used for the case of no zonal winds. This model run is hereafter referred to as the *solstice zonal winds* case. The mode period was found to be 5.30 days as compared to 5.40 days in the case of no zonal winds. Comparing Figs. 7 and 6, we see that in the presence of solstice zonal winds there is a very large amplitude response in the summer mesosphere. The behavior of the wave phase suggests the presence of a standing wave at these levels. Our interpretation is that the mode becomes locally propagating in the region of the easterly jet in the mesosphere and upper stratosphere and is vertically trapped by the weak winds at greater altitudes. In contrast to this behavior, the mode amplitude in the winter hemisphere decreases rapidly through the strong winter westerly jet and is much reduced in the winter mesosphere compared with its amplitude there in the case of no zonal winds. The asymmetry of the response in the troposphere when solstice zonal winds are present is very small. In both hemispheres the rate of decay with altitude through the troposphere and lower stratosphere is reduced relative to that of the no zonal winds case. This relatively slow decay appears to result from the negative temperature gradient at the lower boundary in both hemispheres as further evidenced below.

Fig. 8 shows the phase and amplitude of the wave temperature field in the solstice zonal winds case. The amplitude is relatively large at high levels and in the summer hemisphere, where it reaches a maximum value of 14 K at about 70 km. The amplitude of the components of the wave motion field are shown in Figs. 9 and 10. The wind direction reverses its phase by 180° in the vicinity of the zero amplitude lines. The wind pattern in the troposphere and most of the stratosphere is close to that which is obtained without zonal winds. In that case (not shown here), the zonal component of the wind is opposite in sign in the tropics, from that of high latitudes, and has zeros at roughly 40° latitude; and the meridional component is antisymmetric with respect to the equator. Figs. 9 and 10 show that the distortion of this pattern by solstice zonal winds is large in the mesosphere (i.e., above $z=7$). Amplitudes are also large at these upper levels, reaching 16 m $s^{-1}$ in the summer hemispheres.

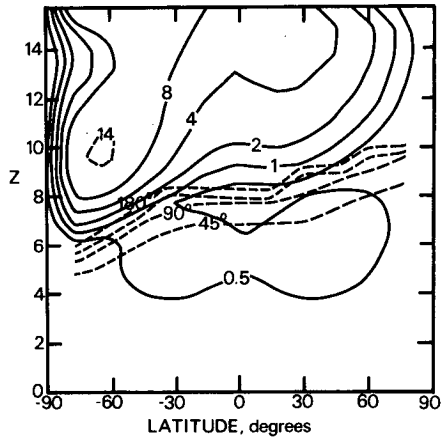


FIG. 8. Amplitude (K) of temperature in solstice zonal winds (solid contours) and phase of temperature in solstice zonal winds (dashed contours).

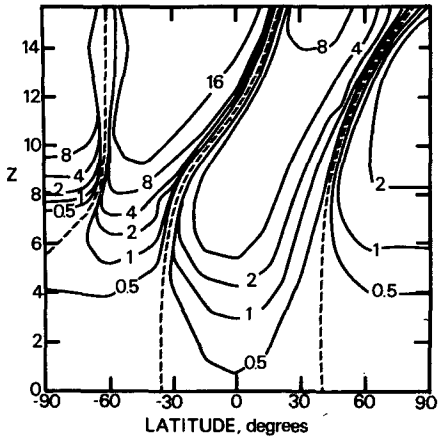


FIG. 9. Amplitude (m $s^{-1}$) of zonal component of wave velocity field $u'$ in solstice zonal winds.

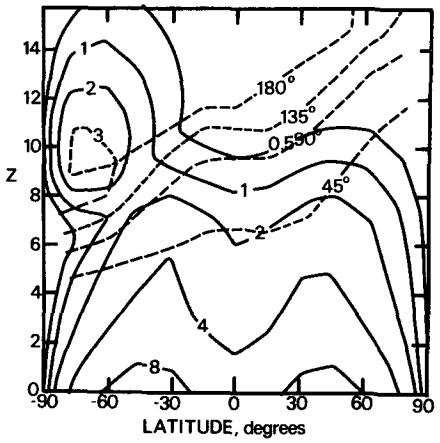


FIG. 11. Amplitude (m) of $h$ in solstice zonal winds when dissipation is present (solid contours) and phase of $h$ in solstice zonal winds when dissipation is present (dashed contours).

To get some idea of the effect of dissipation on the mode in general and on the summer mesosphere standing wave in particular, we ran the model with a damping proportional to the wave temperature field. This *Newtonian cooling* models the damping due to infrared radiation if the coefficient of proportionality is a function of altitude, empirically determined, as for example in Dickinson (1973). It was not convenient with the computational scheme described in Section 2 to include a variation with altitude in the Newtonian cooling coefficient without major revision of the program and so we used at all altitudes a typical value of 10 $days^{-1}$. Phase and amplitude of the height field for this case are shown in Fig. 11, where it can be seen that the principle effect of such dissipation is to reduce by a factor of 2 the maximum amplitude of height perturbation in the summer mesosphere.

The importance of the horizontal temperature gradient term in the lower boundary condition can be inferred by comparing Fig. 7 with Fig. 12, which shows the amplitude of $h$ in a model run where the zonal wind and its derivatives are included but the temperature gradient term is omitted from the lower boundary condition. The case with no lower boundary temperature gradient is characterized by relatively rapid decay of the solution in the troposphere and stratosphere and by a significant asymmetry at low levels. The period of the mode decreases from 5.30 to 4.90 days.

In the presence of equinox zonal winds the pattern of contours of the amplitude of $h$ is symmetric with respect to the equator and looks very much like that in the no zonal wind case (Fig. 6). The only differences are a slightly lower rate of decay with altitude in the troposphere and lower stratosphere due to the negative temperature gradient at the lower boundary and a slightly faster rate of decay with altitude in the upper stratosphere and in the mesosphere due to westerly zonal winds there.

Some idea of the sensitivity of mode structure and phase speed to zonal wind variability can be obtained

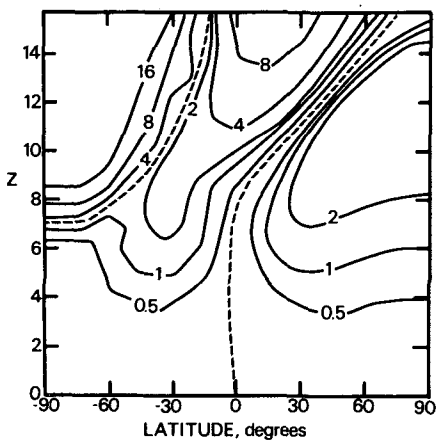


FIG. 10. Amplitude (m $s^{-1}$) of meridional component of wave velocity field $v'$ in solstice zonal winds.

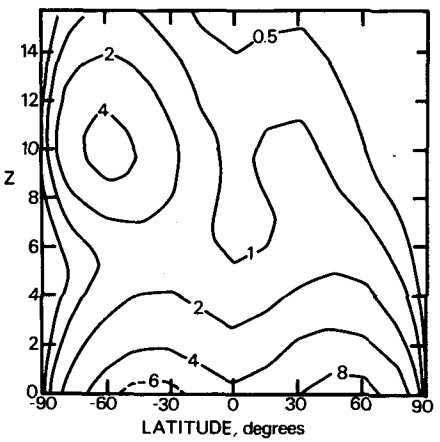


FIG. 12. Amplitude (m) of $h$ in solstice zonal winds when horizontal temperature gradient is omitted from lower boundary condition.

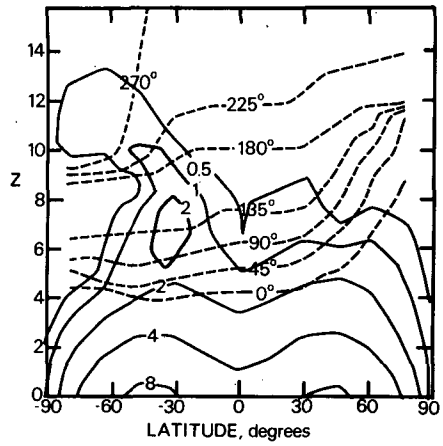


FIG. 13. Amplitude (m) of $h$ when solstice zonal winds are scaled by a factor of 1.4 (solid contours) and phase of $h$ when solstice zonal winds are scaled by a factor of 1.4 (dashed contours).

by comparing model runs with different zonal wind configurations. We ran the model with the zonal wind (and temperature gradient in the lower boundary) everywhere scaled by a factor of 1.4 and by a factor of 0.6, hereafter referred to as *strong* and *weak* solstice zonal wind cases. Mode period is increased by 0.10 day and decreased by 0.05 day in the respective cases. Amplitude and phase of the height field variable $h$ in the strong solstice zonal wind case are shown in Fig. 13. Comparison with the $h$ field in the typical wind case (Fig. 7) shows that in strong winds the summer mesosphere cavity is detuned and amplitudes are only a factor of 2 larger there than at the same levels in the winter hemisphere, as opposed to the order of magnitude difference indicated in Fig. 7. Amplitude and phase of the height field variable $h$ in the weak solstice zonal wind case is shown in Fig. 14. In weak winds the structure more nearly resembles the external normal mode structure that exists in the absence of zonal winds, but the amplitude in the summer mesosphere remains as large as it is in the case of typical solstice zonal winds.

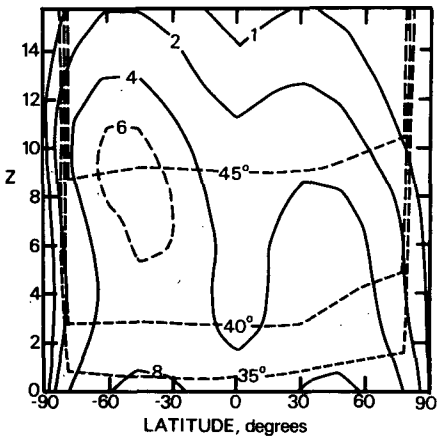


FIG. 14. As in Fig. 13 except for a scaling factor of 0.6.

The model was then run for numerous values of the zonal wind scaling factor in the interval from 0 to 1.4 to explore the variation of the amplitudes in the summer mesosphere with zonal wind strength. Results of this experiment are summarized in Fig. 15, where we show maximum temperature in the mesosphere ($7 \leqslant z \leqslant 12$) as a function of zonal wind scaling factor. The largest response occurs for a scaling factor of 0.7. It turns out, however, that the amplitude of $h$ at the upper boundary of the model for this run is only a factor of 2 smaller than the value at the lower boundary. The rigid lid upper boundary condition may then be influencing both the value of scale factor at which the resonance occurs as well as the structure of the solution. Results for model runs with the Newtonian cooling coefficient of 10 days$^{-1}$ are represented in Fig. 15 by crosses. These show that this dissipation broadens the maximum temperature response—and reduces its magnitude to about 10 K. This dissipation also reduces amplitudes at the upper boundary to values more than an order of magnitude smaller than values at the lower boundary. The variation of mode period with wind strength for the nondissipative runs went as follows: The period decreased from its value for no winds (5.3 days) down to 4.9 days for the zonal winds which gave the largest response and then slowly increased from there with further increase of wind strength.

## 4. Summary and conclusions

From the behavior of the amplitude of the height field variable $h$, we can summarize the effect of zonal winds and the associated temperature gradient at the lower boundary on the structure of the 5-day wave as follows. When there are no zonal winds (Fig. 6), $h$ decays exponentially with altitude (external mode

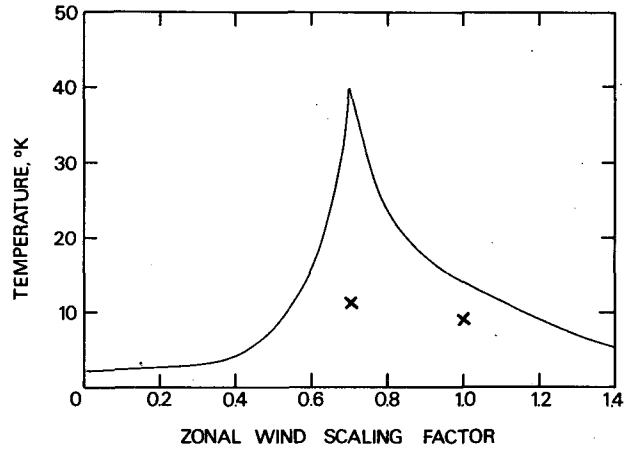


FIG. 15. Maximum amplitude (°K) of temperature wave in the summer mesosphere as a function of zonal wind scaling factor (solid line). Same quantity in model runs when dissipation is included is denoted by crosses.

vertical structure) and is symmetric with respect to the equator. The same structure prevails in equinox zonal winds except for slight differences in vertical decay rate due to the temperature gradient at the lower boundary and moderate westerly winds in the mesosphere. Proceeding to the case of solstice zonal winds (Fig. 7), we find a large asymmetry in the mode structure due to the existence of a wave cavity in the summer mesosphere and a rapid decay of amplitude in the winter mesosphere. The mode exhibits no significant asymmetry in the lower atmosphere, apparently because structure changes due to the temperature gradient at the lower boundary cancel those due to the zonal wind configuration (compare Figs. 7 and 12).

The temperature field of the 5-day wave in solstice zonal winds is shown in Fig. 8. As with other figures in this paper the amplitude has been determined by scaling the solution to give a surface pressure wave of 1 mb amplitude, which is a lower limit of the 1–2 mb value estimated from observations (Madden and Julian, 1973). The mesospheric cavity is tuned to give maximum response of 40 K for solstice zonal winds scaled by 0.7, but with dissipation included the resonance is very broad and peak amplitude of the summer mesosphere temperature wave is reduced to about 10 K (Fig. 15).

The effect of zonal winds and the associated temperature gradient at the lower boundary on the period of the 5-day wave is rather small. Our model indicates that this results from an almost exact cancellation between the tendency of the zonal winds to increase the westward angular velocity of the mode and the tendency of the temperature gradient at the lower boundary to decrease the westward angular velocity. This confirms a suggestion made previously on the basis of a $\beta$-plane analysis (Geisler and Dickinson, 1975). The reader is referred to this earlier paper for an interpretation of zonal wind and lower boundary temperature gradient influence on external mode phase speed in terms of basic state potential vorticity gradients.

*Acknowledgments.* This research was supported in part by the National Science Foundation under Grant GA 37208. The authors wish to thank R. Garcia for certain aspects of the programming and R. Sweet for assistance with the block-tridiagonal matrix inversion. Thanks also to R. Madden for reading the manuscript.

## REFERENCES

Dickinson, R. E., 1973: Method of parameterization for infrared cooling between altitudes of 30 and 70 kilometers. *J. Geophys. Res.*, **78**, 4451–4457.

Geisler, J. E., and R. E. Dickinson, 1975: External Rossby modes on a $\beta$-plane with realistic vertical wind shear. *J. Atmos. Sci.*, **32**, 2082–2093.

Holton, J. R., 1975: *The Dynamic Meteorology of the Stratosphere and Mesosphere. Meteor. Monogr.*, **15**, No. 37, 216 pp.

Lindzen, R. S., and D. Blake, 1972: Lamb waves in the presence of realistic distributions of temperature and dissipation. *J. Geophys. Res.*, **77**, 2166–2176.

——, and S. Hong, 1974: Effects of mean winds and horizontal temperature gradients on solar and lunar semidiurnal tides in the atmosphere. *J. Atmos. Sci.*, **31**, 1421–1446.

Longuet-Higgins, M. S., 1968: The eigenfunctions of Laplace's tidal equations over a sphere. *Phil. Trans. Roy. Soc. London*, **A262**, 511–607.

Madden, R. A., and P. A. Julian, 1972: Further evidence of global-scale 5-day pressure waves. *J. Atmos. Sci.*, **29**, 1464–1469.

——, and ——, 1973: Reply to comments on "Further evidence of global-scale, 5-day pressure waves." *J. Atmos. Sci.*, **30**, 935–940.

——, and J. Stokes, 1975: Evidence of global-scale 5-day waves in a 73-year pressure record. *J. Atmos. Sci*, **32**, 831–836.

Moura, A. D., 1976: The eigensolutions of the linearized balance equations over a sphere. (Submitted to *J. Atmos. Sci.*)

Robert, A. J., 1969: Integration of a spectral model of the atmosphere by the implicit method. *Proc. WMO/IUGG Symposium on Numerical Weather Prediction*, Tokyo, 26 November–4 December 1968, Japan Meteor. Agency.

——, J. Henderson, and C. Turnbull, 1972: An implicit time integration scheme for baroclinic models of the atmosphere. *Mon. Wea. Rev.*, **100**, 329–335.

Rodgers, C. D., 1976: Evidence for the five-day wave in the upper stratosphere. *J. Atmos. Sci.*, **33**, 000–000.

Taylor, G. I., 1929: Waves and tides in the atmosphere. *Proc. Roy. Soc. London*, **A126**, 169–183.

Tsay, C.-Y., 1974: Analysis of large-scale wave disturbances in the tropics simulated by an NCAR general circulation model. *J. Atmos. Sci.*, **31**, 330–339.